Modeling of Quasi-Parallel Fiber Networks at the Microscopic Scale

O. Haji, X. Song, Audrey Hivet, S. Rolland Du Roscoat, L. Orgéas, A. Sinoimeri, G. Hivet, E. Blond

MODELING OF QUASI-PARALLEL FIBER NETWORKS AT THE MICROSCOPIC SCALE

O. Haji[a], X. Song[a*], A. Hivet[a], S. Rolland du Roscoat[b], L. Orgéas[b], A. Sinoimeri[c], G. Hivet[a], E. Blond[a]

[a]Laboratoire de mécanique Gabriel LaMé, EA7494, université d'Orléans, université de Tours, INSA Centre Val de Loire, 8 rue Léonard de Vinci, 45072 Orléans, France.

[b]CNRS/Université de Grenoble-Alpes, Laboratoire Sols Solides Structures Risques (3SR),UMR 5521, BP 53, 38041 Grenoble cedex 9, France.

[c]Université de Haute Alsace, Laboratoire de Mécanique et Physique Textiles 11, rue Alfred Werner, 68093 Mulhouse, France.

[*]Corresponding author: X. Song (xinling.song@univ-orleans.fr).

Abstract

The understanding of the mechanical behavior of quasi-parallel fibers network is an important issue for the development of the manufacturing processes of fibers reinforced composite materials. This study presents a numerical model of quasi-parallel fiber networks, which consists of a realistic representation of the fiber network geometry, and a reliable simulation strategy to reproduce the main phenomena at the fiber scale. To obtain feedback on this approach, experimental compaction was performed on a bundle of polyester fibers. The experiment was combined with X-ray tomography scans of the specimen to extract the initial state and use it to create a CAD model, implemented in finite element simulations. Each fiber is modeled by 3D linear beam elements, and the contact law between the fibers is based on the Hertz contact model taking fiber friction into account. The comparison between numerical and experimental show good coherence, demonstrating the potential of the strategy.

Keywords

Fibers, Finite element analysis (FEA), Mechanical testing, X-ray tomography

Data Availability Statements

All data generated or analysed during this study are included in this published article (and its supplementary information files).

Statements and Declarations

Competing of Interest

The authors declare that they have no known competing financial interests or personal relationships that could have appeared to influence the work reported in this paper and the publication of this article.

Acknowledgments

This work project was supported by the China Scholarship Council (CSC), the project of "National constructed high-level university-sponsored graduate programs" (Funding number: 202008120116).

The authors also thank ANR AMOC and Tec21 for their support.

Introduction

The improvement of fibrous reinforced composite manufacturing processes is required in terms of cost, quality, and productivity rate. For instance, RTM (Resin Transfer Molding) is a closed-molding fabrication process that allows for automatic, high-quality and cost-effective production. The first step in the RTM process consists in performing a dry fibrous textile before injecting the resin. Depending on the desired shape of the final part, the fibrous textile undergoes different mechanical loads, which induce strains and damage to the fabric. As a result, the mechanical properties of the final parts are drastically impacted. It is therefore essential to predict the preforming process of composite parts and optimize the fabrication parameters. Two main approaches are possible to achieve this task: an experimental or a numerical approach. However, proceeding with experimental tests until the optimum parameters are found is long and expensive compared with an approach based on numerical simulations. In order to simulate the performing process, it is necessary to establish an appropriate mechanical behavior of the fibrous textile. This behavior is mainly a structural effect that depends essentially on the yarn interlacing and secondly on yarn behavior. Each yarn is composed of thousands of fibers, each of which can be considered a homogeneous material. Therefore, the reinforcement's behavior depends on both the behavior of the fibers and their interactions inside the yarn. Consequently, the fiber scale can be considered the finest one to understand and model the reinforcement behavior. This task would be quickly and simply achievable by establishing a reliable numerical model at the fiber scale to model the fibers' behavior and their interactions. Technical yarns with adjacent, quasi-parallel fibers are mostly used in the manufacturing of fibrous reinforcement composite materials. The main objective of the present paper is to develop a thorough numerical methodology to simulate the deformation of these types of fiber networks as they undergo different loading paths during the performing step. This approach will provide an extensive database for establishing yarn behavior at the mesoscopic scale, and then the fabric behavior at the macroscopic scale. The focus of this study is on the compaction load path, as it is the most representative complicated load path leading to fiber rearrangement, while others, such as tension lead to fiber deformation.

The mechanics of fibrous networks has been investigated in many experimental studies, for instance [1] discusses the character of the structure, [2] studies the compression with a maximum load of 100N, and [3] with a maximum compression load of 600N. They concluded that the mesoscopic response of fiber assemblies is non-linear and non-reversible due to fiber deformations, frictional sliding and irreversible rearrangement within the fiber assembly. These experimental studies have been confirmed by X-ray tomography, which has also been used to characterize compaction, taking advantage of the local 3D representation of the fiber assembly [4] [5]. Experimental studies have been crucial to explore different approaches to the behavior of fibrous media, for instance [6] [7].

From a numerical perspective, the compaction of fiber networks has been studied by two main approaches: rigid element simulations based on molecular dynamics and finite element simulations. Rodney et al. [8] used the first approach to model the compaction of quasi-parallel fibers; potential energy was used to model the fiber behavior. It took into account traction, bending stiffness, and the contact interactions between fibers. The non-penetration condition was included, but the friction coefficient was neglected. Based on this model, Rodney et al. were able to predict both the number of contacts per fiber, corresponding to the packing density and the energy per fiber as a function of the relative density. In a subsequent study, friction interactions were added to the model [9], and showed that friction shifts the densities to lower values. Subramanian and Picu [10] also used models based on molecular dynamics. Unlike the previous model in which the contact energy was defined by a Hertz potential, Subramanian and Picu defined the contact energy as a repulsion potential. They concluded that inter-penetration and sliding at contact points are the prevailing phenomena during the final steps of compaction. In addition, they both decrease as the friction coefficient increases.

The following other studies modeled fibers by using different types of bar and beam elements. In [11], a fiber network model was developed with arbitrary initial orientation, fibers were modeled by beam elements with constant curvature, and the interactions at the contact points were provided by springs. The results showed a good agreement with the experimental tests. However, the fiber volume fraction was limited to 3% and the numerical model was limited to geometrically linear deformations. A recent study proposed a model of uniaxial compaction of quasi-parallel fiber networks [12]. The fiber assembly

was represented by a periodic unit cell in which each fiber was modeled by straight beam elements. This model was used to investigate the effect of simulation parameters, such as contact damping, material damping, and friction coefficient on the accuracy and robustness of calculations. Both the packing stress (i.e. the component of the stress tensor along the compaction direction) and the number of contacts corresponding to a friction coefficient of μ=1 were compared to those of van Wyk's [13] and Toll's [14] studies because they are based on the no sliding assumption. However, the results obtained for a meaningful friction coefficient were not compared to experimental data. Durville [15] [16] also obtained results in accordance with those of van Wyk using the Cosserat beam theory. His model was enhanced by a penalty law to manage fiber penetrations at the contact zones. For friction, the Coulomb law was adopted. He also estimated the number of fiber contacts Nc with respect to the fiber volume fraction v_f : $Nc \propto {v_f}^{2/3}$.

Mathematical-computational approaches have also been used to study the compaction of fiber networks, N.Beil developed a fiber assembly model [17] [18] [19], and used it to simulate uniaxial compaction. The model contained fifty helix-shaped fibers randomly implemented in a unit cell. The fiber behavior was modeled by the Bernoulli-Euler theory of elastic rods. In addition, both repulsion and frictional forces were used to model interactions at fiber contact points. The model made it possible to investigate, for instance, the evolution of the pressure on the fiber assembly as it undergoes a loading-unloading cycle, the number of contacts between the fibers, the interaction forces at the contact points, and the fiber crimp effect. However, the previous fiber network compaction features were obtained at a low fiber volume fraction range ($\varphi_0 = 0.8\%$) [17].

To summarize, the numerical studies cited above investigated some of the important microstructural parameters, such as packing density, fiber contacts, fiber penetration, initial orientation, fiber curvature, and friction coefficient, that are useful to extend our understanding of the mechanical behavior of fibrous media. However, these studies were not compared with experimental data, which is crucial to validate the numerical results. For this reason, recent studies have attempted to take the lead in the numerical/experimental dialogue and compare their numerical results with experimental data. Daelemans et al [20]. describe a solution that enables predictive compressive simulations through hybrid

virtual fibers. The authors simulated the compression of twill fabric layers with hybrid virtual fibers having bending stiffness based on the virtual fibers developed by the Dynamic Fabric Mechanical Analyzer (DFMA). The effect of the number of virtual fibers and the length-to-diameter ratio on the simulation results is discussed. However, most of these studies do not investigate in depth the mechanical behavior of yarns with quasi-parallel fibers. In fact, very few numerical studies have been carried out on unidirectional fibrous media [21] [22] [23] [24] [25]. Moreover, they did not attempt to model the yarn behavior. Furthermore, in [25], the friction coefficient between fibers was just identified to fit the experimental results. In addition, this study differs from [26] [27] [28], by the use of different numerical strategies. In these studies, the authors made the choice to use digital elements: bar elements linked by rigid knots. Whereas, in the present work, the choice was fixed on beam elements, on the one hand, because their potential was highlighted by other previous studies. On the other hand, the linear beam elements (B31) allow handling well the problems of a large number of contacts by using the general contact algorithm on Abaqus/Explicit. In addition, the experiment/simulation comparisons of the compaction curves encourage their use. Considering the following steps of the predefined approach, a significant gain is expected from the beam elements, especially in terms of computation time.

The objective of the present study is to fill this gap in the literature and offer a quasi-parallel fiber network model with a reliable simulation strategy. This model is intended to simulate, comprehend and model the mechanical behavior of fiber yarns. The model is validated by theoretical and numerical test cases, and most importantly, it is compared with experimental results. The comparison is even more meaningful as the geometry model of the fiber assembly is representative of the real microstructure geometry, which is not the case for previous studies. Such a numerical model requires: (i) a realistic representation of the fiber network geometry and (ii) a reliable simulation strategy to model the main phenomena at the fiber scale. To feed this approach, compaction tests were conducted on fiber network specimens. The experiments were combined with X-ray tomography image analysis in order to: (i) extract the initial microstructure of the fibrous specimen before starting the compaction test; (ii) monitor the intermediate microstructure evolution at different stages of the experiment.

The originality of this work is characterized and modeled the behavior of a fibrous medium at the micro-scale. In addition, the proposal of a dialogue between an experimental approach and a numerical one

throughout the development and validation process of the simulation strategy. The numerical tests were performed on the same initial microstructures of the fibrous samples thanks to the use of X-ray tomography. This enhances the credibility of the validation process. This microstructure representation was enriched by data collected during compaction (load, displacement, and X-ray images of the specimen).

1. Experimental and numerical tools

1.1. Experimental tools

A non-saturated specimen of polyester fibers ($E \approx 15\ GPa$) was prepared for the compaction test. The fibers were initially curved because they were wound on a cylindrical spool. The specimen consists of 40 fibers. The number of fibers was purposely limited because it is easier to characterize a fiber network behavior with fewer fibers rather than with numerous fibers. In addition, since establishing and validating a simulation strategy requires running a large number of simulations, a limited number of fibers is more beneficial to obtain practical CPU times. Each fiber has a diameter of $\emptyset = 0.5mm$ and a length of $l = 15mm$, the 3D maps of the real specimen as shown obtained by FIJI software in the figure 1(a).

The specimen was subjected to a uniaxial confined compaction test, i.e. the lateral surfaces are not stress-free. For this purpose, the fibers were placed on a rectangular plate (width=3mm, length=6mm as presented in figure 2(a)) which is fixed on a micro-press designed in the 3SR laboratory in Grenoble [5]. The micro press consists of two plates: (i) the rectangular one, which contains the fibers, and is connected to a micro-motor; the compaction is controlled by a displacement U; (ii) the upper plate is connected to a load cell (capacity = $50N$) in order to record the compaction load F. The micro-press was placed on a micro-tomograph in order to scan the specimen at different compaction steps. 3D X-ray microtomography images, with the pixel size of $r = 15\ \mu m^3/voxel,$ tube tension of $100KV$ and tube intensity of $100\mu A$, were thus obtained and were post-processed to reconstruct the specimen microstructure. The reconstructed 3D maps were used to obtain the skeleton of the specimen microstructure by uniformly reducing the fiber radius, in which each fiber is represented by its mid-line (Figure 1(b)). They can therefore be modelled by 3D beam elements. Before starting compaction, the specimen was carefully placed in contact with the upper plate without changing the position of the fibers, and then it was scanned

to obtain the initial microstructure. The specimen was compacted afterward. As the test progresses, the load cell records the compaction load. The compaction was interrupted whenever a significant change in the fiber positions was observed, so the relationship between loading force and time is stepwise. The total compaction experiment time is 30519.159s (508.65 min), which includes the upward movement time of the mandibular plate and the scanning time of the X-ray Tomograph. These interruptions are useful for two reasons: (i) measuring the plate displacement U and the corresponding load compaction F during the different stops in order to deduce the mechanical response of the fiber assembly as displayed in figure 2(b); (ii) rescanning the specimen's microstructure and to obtain later the fiber positions at different steps, the curve of compression loading force with time is shown in Fig. 2(c). The compaction test above and its corresponding image analysis constitute the database that was then used to validate the numerical model via an experimental/numerical comparison.

1.2. Numerical tools

The present section introduces the methodology followed to define the simulation strategy regarding the computation convergence, reliability and efficiency. The simulations were performed on Abaqus/ Explicit because it is more suitable for this type of study in terms of convergence, contact algorithms and total CPU time. All the simulations in the present paper were executed using an Intel® Xeon® machine (CPU E5-1650 v3, 3.5GHz).

2. Numerical procedure

Two main categories of elements are potentially usable: deformable finite elements and rigid discrete elements. As the fibers are initially curved, fiber deformation, especially bending, is one of the contributing factors to the fiber network compaction behavior. For this reason, finite elements appear to be an adequate choice. While the present study used 40 fibers for validation purposes, the approach adopted in this study is defined in two steps: the first one consists in defining a simulation strategy that will allow reproducing in an efficient and reliable way of the physical phenomena occurring during compaction. The validation of this simulation strategy will allow its use in the second step which consists in setting up a model of a hundred fibers to understand and model the law of behavior of entanglement of quasi-parallel fibers. During the first step presented in this paper, experimental and numerical tests

were performed to define the parameters of the simulation strategy, they were then validated by an experiment/simulation dialogue. The process of definition and validation of these parameters requires several numerical tests and data post-processing whose execution time depends on the number of fibers, hence the use of a limited number of fibers. This will allow performing the necessary and enough tests to identify the parameters of the simulation strategy while reducing the computation and post-processing times. On the other hand, this approach allowed to validate the ability of the simulation strategy to faithfully reproduce the physics of compaction on a limited number of fibers. It is easier to increase the number of fibers later to work on a model representative of real cases.

3.1 Finite elements

Thus, each fiber was modeled by 3D beam elements, as these types of elements are geometrically simple (one-dimensional line) and contain a small number of integration points (three at most for the cubic beam elements). In the process of mechanical analysis, it is generally divided into Timoshenko beams and Euler beams. Timoshenko beams (B21, B22, B31, etc.) consider bending deformation as the main deformation and shear deformation as the secondary deformation, which are flexible beams and more suitable for slender components. Therefore, it is more suitable for simulating fiber assemblies. Linear interpolation beam elements (i.e. B31 elements) are more suitable for simulations involving contacts [29], which is the case for fibrous media. They were therefore used in the present study. As mentioned earlier, fiber bending is as important as contacts, especially for initially curved fibers. Therefore, each fiber must be sufficiently meshed to avoid any misrepresentation of the fiber's deflected shape.

3.2 The contact behavior of beam elements.

Concerning the real fibers of the compacted specimen, increasing the contact forces can generate a local strain as illustrated in figure 3(b), especially in the static phase. In the quasi-parallel fibers network, the main contact between the two fibers is oblique. Therefore, the resulting contact is localized. In addition, during compaction, the rearrangement of fibers is mainly observed and the contact force between fibers does not reach local deformation, so the local deformation is negligible. In this case, the contact stiffness depends on the deformability of the fiber cross section. However, as beam elements are based on the assumption of a rigid cross-section, the beam cross sections penetrate each other,

generating a penetration depth, denoted δ, instead of a local strain (cf. figure3(a)). For this reason, the aim of the present part is to provide a contact stiffness for beam elements that is sufficiently close to the contact stiffness obtained by deformable sections. Since the cross-section of beam elements is rigid, the local deformation was omitted, considering only the penetration between fibers in contact with each other. Then, the relationship between the penetration depth δ and the contact force is controlled through a Hertz contact model.

From a numerical perspective, Abaqus provides contact force-penetration relationships to define a contact model. Since the Hertz contact curve can be fitted by a power function, the suitable contact relationship would be a linear interpolation (n segments, i ϵ [1, n]) of a power function between the contact force and the penetration depth as presented in figure 4 [29]. d is interpolation step, δ_i and K_i respectively the current penetration and the current stiffness at the segment i and K_{deff} the default contact stiffness. Each time the current penetration δ_i exceeds a multiple of the penetration measure d (i.e. $\delta_i \geq id$), the contact stiffness K_i is scaled by a factor S. The initial stiffness is set equal to the default contact stiffness K_{deff} multiplied by a factor S_0. Consequently, for each current penetration δ_i in the segment $[(i-1)d\ , i\ d$, the stiffness K_i is expressed by equation 1. The simulation contact model is then identified using the parameters S, S_0 and d.

$$K_i = S_0 K_{def} S^{(i-1)} \qquad (i = 1, 2, 3 \cdots \cdots n) \text{ [29]} \tag{1}$$

The specimen used in the present study is a quasi-parallel fiber network. Therefore, two types of fiber contact configurations could potentially be formed: (i) Parallel fiber contact where the contact area is rectangular (cf. figure 5(a)); (ii) Oblique fiber contact with a relative fiber orientation Φ (cf. figure 5(b)) and an elliptic contact area. For the second case, the contact force-penetration relationship depends necessarily on the relative fiber orientation Φ, which changes eventually for every two fibers in contact as the compaction progresses. However, the contact formulation provided by Abaqus does not consider this change in orientation. Instead, it identifies only one constant orientation. Hence, two extreme relative orientations and an average value between them were tested independently: $\Phi_1 = 2°$, $\Phi_2 = 6°$, and $\Phi_3 = 10°$, using the contact model described earlier. Parallel and oblique contact forces between two fibers modelled by B31 elements are plotted respectively in figures 5(a) and 5(b) as a function of the

penetration depth δ for each relative orientation. Each contact force is modelled by Hertz's law for parallel and oblique cylinders [30] [31] [32]. It can be observed that the numerical contact model accurately reproduces the analytical contact models (n ≈1000). Therefore, the assumption adopted here of controlling the contact stiffness through the penetration depth δ seems reasonable.

However, the relative orientation change between every two fibers is costly in terms of realization and CPU time. An alternative solution could be to identify one average relative orientation, and then apply it to the entire fiber network. This alternative is available only if some orientations are simulated independently, and each one of them offers similar compaction curves. For this reason, the identified relative orientations Φ_1, $\Phi_2 = \Phi_{average}$ and Φ_3 were used to simulate the compaction test. The three simulations were also compared with the compaction curve obtained by the parallel contact model ($\Phi_0 = 0$). The simulations were performed using the simulation strategy developed in this paper. The parameters used and the identification curves are given in table 1 and figure 6. The results obtained are displayed in figure 7 where the compaction load is plotted as a function of the displacement U used to control the compaction test. During the fiber rearrangement phase, the three relative orientations do not influence the global compaction behavior because the compaction load is not yet significant. However, the final compaction load depends on the contact relative orientation. As shown in the figure 7, the final compaction load for the parallel contact model (17 N) is 44% higher than the oblique contact load (9.5 N) (for $\Phi_2 = \Phi_{average} = 6°$). In fact, as explained earlier, the fibers are not all parallel, for example, in the figure 1; a certain percentage of oblique fiber contacts is always present in the fiber network and it must be taken into consideration, and vice versa when considering only the oblique fiber contact.

3.3 Theoretical and numerical benchmarks

The aim of this section is to present the analytical and numerical test cases used to identify accurate and reliable simulation parameters. The advantage of these test cases is that they are simple but crucial, and their reference solutions can be calculated analytically or obtained numerically. At the same time, they are also useful to gather meaningful and efficient information about the static and the kinematic behavior of the fibers in a reasonable CPU time.

3.3.1 The dynamic phase: fiber rearrangement test case

Fiber rearrangement is an important phenomenon at the fiber scale because it reflects the effect of friction on the fiber kinematics. For this reason, the compaction experiment was performed at a low velocity ($v_{test} \approx 5.22mm/min$) to ensure a quasi-static test and avoid inertia effects, which could modify the fiber kinematics. From a numerical perspective, the simulation strategy must also provide quasi-static simulations. Therefore, a test case based on the rearrangement phase of the compaction test was developed and used to identify the appropriate parameters to ensure a quasi-static simulation. The test case attempts to study the rearrangement of three beams placed on an analytic rigid plate as displayed in figure 8. The upper beam is subjected to a displacement u_z along the z-axis. Then the displacements u_{y2} and u_{y3} along the y-axis are calculated respectively for the other two beams (2 and 3) as a function of u_z. A friction coefficient of $\mu = 0.2$ was used. This value was estimated experimentally using polyester fibers [33]. Since the analytical solution for such cases is not evident, an implicit dynamic analysis in Abaqus/Standard was used instead as a reference solution for the present test case. The results are automatically checked for accuracy in Abaqus/Standard analysis [29] since it is based on an implicit integration schema and the equilibrium equation is solved at every time increment. The displacements u_{y2} and u_{y3} obtained for beams 2 and 3 were considered as a reference to validate those obtained by the dynamic explicit analysis. Since the test case model is symmetric relative to the plane $(S, \vec{x}, \vec{z})$ (cf. Figure 8), only the displacement $u_y = u_{y2} = -u_{y3}$ is plotted. The results of the reference solution are presented on figure 9 where the displacement u_y along the y-axis is plotted versus the displacement u_z, and on figure 8(b) where the final configuration of the beams is displayed. It can be observed that beam 1 remains in contact with beams 2 and 3 at the end of the simulation.

The CPU time needed to run a quasi-static analysis can be very long using an explicit schema as the simulation cost is proportional to the number of time increments n, which is expressed as follows:

$$n = T.\max\left(\frac{1}{L_e}\sqrt{\frac{\lambda + 2\mu}{\rho}}\right) \quad (2)$$

Where T is the time period of the simulation, L_e is the finite element size, λ and μ are the effective Lamé constants and ρ is the material density. A quasi-static event needs, naturally, a long time period T. In addition, linear beam elements (B31) are used (cf. section 3.1), so the mesh size used L_e is small ($L_e =$

$0.3mm$ corresponding to 50 elements per fiber) to properly simulate fiber bending. Therefore, according to equation 2, more time increments are needed in the present analysis, increasing the computational cost. The test case described earlier was used in order to illustrate this phenomenon. Different time periods T were tested, i.e. different velocities v_z were tested from $v_z = \frac{u_z}{T}$, where u_z is the displacement applied on beam 1. It was concluded that a velocity of $v_z = 0.23mm/min$ enables exactly the same displacements to be obtained as with the reference solution, as displayed in figure 10(a). However, the simulation time is unacceptably long (≈12 hours) for only three beams. At this stage, it is worth asking how the fiber rearrangement in Abaqus/Explicit can be properly simulated in a reasonable CPU time. This is the objective of the present step of the simulation strategy development.

Based on equation 2, two classical procedures can be used: Increasing the material density ρ, or artificially reducing the time period T (i.e. increasing the loading velocity). Increasing the material density is not suitable because it will induce a change in the equilibrium of the fibrous assembly in the initial state: the higher the density, the more the microstructure is impacted by the gravitational and internal field. Therefore, the fibers' initial positions are no longer the same as in the real specimen. For this reason, reducing the time period T was adopted in the present study. A reasonable CPU time, e.g. a couple of hours, must be targeted in view of the longer-term objectives of the study of using fiber assemblies with hundreds of fibers. Preliminary simulations of the compaction test, which consists of 40 fibers, were performed and it was concluded that a loading velocity in the range of $10^3 mm/min$ gives a CPU time of a couple of minutes, which is reasonable to reach the target CPU time. $v_z' = 10^3 mm/min$ was tested using the rearrangement test case described earlier. The results are presented in figure 10(a) where the obtained displacement u_y is compared with the reference solution.

Figure 8(c) represents the final configuration of the beams using the velocity v_z'. It can be observed that the simulation is no longer quasi-static since the displacements u_y is not in accordance with the reference solution. Moreover, the beams do not remain in contact with one another as predicted by the reference simulation due to the inertia effects induced. To reduce the effect of inertia, a damping parameter is introduced according to the dynamic equilibrium equation (equation 3). In fact, Abaqus/Explicit is based

on the time integration of this dynamic equilibrium equation using a time increment Δt as expressed in inequality 4.

$$[\mathrm{K}]\, u + [D]\, \dot{u} + [M]\, \ddot{u} = \sum F_{ext} \tag{3}$$

$[\mathrm{K}]$, $[D]$ and $[M]$ are respectively the stiffness, the damping ,and the mass matrices. F_{ext} is the external forces vector.

$$\Delta t \leq min\left(L_e \sqrt{\frac{\rho}{\lambda + 2\mu}} \right) \tag{4}$$

Using a small mesh size L_e, as is the case here, induces smaller increment times. In addition, reducing the time period T automatically increases the loading velocity. On the other hand, integrating the equilibrium equation (equation 3) through small time increments increases the inertia term $[M]\ddot{u}$, especially when increasing the loading velocity, which induces significant inertia effects. For this reason, the inequality 5 must be respected to maintain a quasi-static simulation [29].

$$K_e < 10^{-2}\, S_e \tag{5}$$

where K_e is the kinetic energy and S_e is the strain energy. As explained earlier, the strain energy during the dynamic phase is lower than the kinetic energy. Reducing the absolute velocity $\dot{u}$ using numerical damping is among the options to overcome this problem since material damping generates damping forces that are opposed to inertia forces. Material and contact damping were already used in such cases in a previous study [12]. The values adopted in [12] were tested on the test case above, but they did not reduce the inertia effects. Different material damping coefficients were therefore tested on the same test case to identify the appropriate material damping parameters, and the results obtained are shown in figure 10(b). It can be seen that the resulting displacement u_y is in accordance with the reference solution, and $\alpha = 10^5$ appears to be the appropriate value for the loading velocity $v_z' = 10^3 mm/min$. The strategy for reducing the computational time is essentially to increase the loading speed relative to the speed of the actual test. As a result of this increase, inertial forces appear and change the velocities and fiber paths compared to the actual test. Therefore, damping had to be added to oppose the inertial forces and reduce the speed of fiber movement. Although damping increases the CPU time slightly (table 2), it remains

nevertheless significantly below that of the quasi-static simulation (≈12h), with similar displacements. In addition, the fiber positions in the experiment and simulation are very close after adding damping (figure 10(b)), which proves that adding proper fiber damping during the simulated compaction can control the CPU time cost and the simulation is close to the experimental results. The influence of adding material damping on contact forces in the static phase is discussed in the following section.

3.3.2 The static phase: test case

After studying the rearrangement phase, it is necessary to analyze the behavior of linear beam elements in the static phase. In the compaction experiment, the initially curved beams become straighter and more compressed. This state can be modelled by the test case illustrated in figure 11(a). It consists of three straights parallel beams modelled by B31 elements. The upper beam (beam 1) is in contact with the lower ones (beams 2 and 3). The centerlines of the lower beams are shifted from the centerline of the upper one by an angle β relative to the z-axis (figure 11(a)). The three beams are placed in a rectangular analytic rigid plate to carry out a confined compaction test. Forty polyester fibers have been compacted in order to validate the present simulation strategy. The test will be described forwards in the Experimental benchmark.

According to the obtained compaction test curve (figure 2(b)), the forty fibers of the specimen undergo a total load of 12N. Therefore, the three beams in the test case undergo a total compaction load of $1N$ in addition to their own weight $\vec{w}$. A line-load equal to $\|\vec{q}\| = 0.066N/mm$ (the fiber length is 15mm) is applied on the upper beam along the z-axis.

Let $\overrightarrow{NF}$ and $\overrightarrow{NF'}$ be the normal contact loads applied by beam 1 on respectively beam 2 and beam 3, $\overrightarrow{RF}$ and $\overrightarrow{RF'}$ the reaction forces applied by the analytic rigid plate on respectively beam 2 and beam 3 along the y-axis and the z-axis (cf. figure 11). The main objective of the present test case is to analyze the response of the normal contact loads $\left\|\overrightarrow{NF}\right\|$ and $\left\|\overrightarrow{NF'}\right\|$ and the reaction forces $\left\|\overrightarrow{RF}\right\|$ and $\left\|\overrightarrow{RF'}\right\|$ as a function of the external load $\|\vec{q}\|$. Since the problem is symmetric with respect to the plane $(A, \vec{x}, \vec{z})$, the normal force $\left\|\overrightarrow{NF'}\right\|$ is theoretically the same as $\left\|\overrightarrow{NF}\right\|$. Likewise, the reaction force $\left\|\overrightarrow{RF'}\right\|$ is the same as $\left\|\overrightarrow{RF}\right\|$. The results obtained will be used to verify: (i) the accuracy of contact forces and reaction forces in

the particular case of the static state of the compaction test; (ii) the influence of the material damping coefficient on the contact forces and reaction forces during the static case. The results are compared with the analytical solution of the same test case. In fact, particularly in this case, the normal contact behavior is defined as a "hard contact" to restrict the angle β variation. The test case can therefore be treated as a rigid solids problem. The application a static equilibrium led to determine the magnitude of $\left\|\overrightarrow{NF}\right\|$ and $\left\|\overrightarrow{RF}\right\|$:

$$\left\|\overrightarrow{NF}\right\| = \left\|\overrightarrow{NF'}\right\| = \frac{q+w}{2cos\beta} \tag{6}$$

$$\left\|\overrightarrow{RF}\right\| = \left\|\overrightarrow{RF'}\right\| = \sqrt{(\frac{1}{2}(q+w)tan\beta)^2 + (\frac{1}{2}(q+3w))^2} \tag{7}$$

The numerical evolution of $\left\|\overrightarrow{NF}\right\|$ and $\left\|\overrightarrow{NF'}\right\|$ as a function of $\|\vec{q}\|$ and that of $\left\|\overrightarrow{RF}\right\|$ and $\left\|\overrightarrow{RF'}\right\|$ are plotted in figure 11(b). The numerical results are compared with the analytical ones in both figures. Analytically, as $\left\|\overrightarrow{NF}\right\|$ and $\left\|\overrightarrow{RF}\right\|$ are linearly dependent on the compaction load $\|\vec{q}\|$ (cf. Appendix), the same linearity evolution is predicted by linear beam elements (B31). The test case symmetry is also respected. Quantitatively, the marginal error between the analytical and the numerical values is negligible (cf. figure 11(b)), which means that the material damping used has no impact on the contact forces. The term $[D]\dot{u}$ in the dynamic equilibrium equation (cf. equation 3) is significantly low in the static phase relative to contact forces. Therefore, the damping forces are negligible compared to the contact forces.

3.4 The simulation strategy: summary

The CAD model of the fibrous microstructure is obtained by post-processing the X-ray tomography images of the real fiber network. Each fiber is modeled by 3D beam linear finite elements. The compaction plates are modelled by rigid analytical shells; the upper one is fixed, while the lower one is controlled by a displacement U. The loading velocity is $10^3 mm/min$ to reach a CPU time target of tens of minutes. A material damping coefficient of $\alpha = 10^5$ is used to control inertia effects. The general contact algorithm provided by Abaqus is used for the entire model, with a friction coefficient of $\mu = 0.2$ [33]. The normal contact behavior is defined as a power function between the contact force and the penetration δ. Some assumptions regarding the mechanical and the geometric model must be taken into account: (i) the

friction coefficient between two polyester fibers is difficult to estimate and depends on many variables [33], therefore an average value of 0.2 was used [33]; (ii) the coefficient of adhesion is assumed to be the same as the friction coefficient; (iii) the local strain between fibers is ignored because of the rigidity of the beams' cross-section but its effect on rigidity is embedded in the contact law (cf. section 3.2 equation 1); (vi) the cross-section diameter is considered identical and constant for all the fibers.

4 Results and discussion

The compaction test was simulated using the simulation strategy developed in this paper. As explained in the previous section, both contact cases between the fibers – parallel and oblique contacts **–** take place during compaction (cf. section 3.2). Therefore, the results obtained by both contact models were compared with the experimental ones. The compaction load F as a function of the displacement U is presented in figure 12(a) for the parallel contact case, in figure 12(b) for the oblique contact case and in figure 12(c) for the identified contact model. In order to better understand the fiber behavior, it is interesting to analyze the simulation results from an energetic perspective as well. Figure 13 displays the evolution of the Kinetic energy K_e, penalty work P_w and strain energy S_e of the whole model. The kinetic energy represents the fiber rearrangements, the penalty work is the work done by contact penalties (i.e. contact energy), and since the fibers are initially curved, the strain energy represents the elastic strain of the fibers due to bending.

When the displacement is in the range of $U \in [0,0.55](mm)$, the compaction load of both contact models, parallel and oblique, is too low (≈98% lower than the maximum load). In this compaction phase, the initial fiber fraction ($v_{f0} = 37.7\%$) allows sufficient space for the fibers to move as rigid bodies. The fiber rearrangement in this particular case is characterized by a negligible strain energy relative to the total kinetic energy, as shown in figure 13. Consequently, in this case, the condition ensuring a quasi-static simulation is not respected. However, the identified damping coefficient seems to be adequate to control the fiber rearrangement and stabilize the simulation. As the strain energy remains negligible, the penalty work increases at $U = 0.26mm$, which means that the interaction between fibers, due mainly to friction, increases. For both contact models, starting from a displacement value of $U = 0.55mm$, the compaction load progressively increases, which means that the total stiffness of the fiber assembly increases relative

to the beginning of compaction. In fact, fiber bending begins to take place simultaneously with the fiber rearrangement, as is proven by the increase in the strain energy at the same displacement value ($U = 0.55mm$). At this particular point, all the model energies are at the same level ($Ke \approx Se \approx Pw$), and it marks the beginning of a transition phase ($U \in [0.55,1.12](mm)$) between fiber rearrangement and fiber locking. The locking of fibers is a logical consequence of the relative motion between the fibers. It depends on (i) mechanical parameters: intrinsic (e.g., friction coefficient of the fibers) and non-intrinsic (e.g., loading velocity); and (ii) geometric parameters: fiber orientation, curvature, the distribution of contact points in the fiber network. This distribution allows the transfer of contact forces, which generate relative motion between the fibers. This relative motion leads to a change in the geometric position of the fibers, resulting in the closure of the pores between the fibers and the formation of locking. With increasing compression force, this locking persists or is released by the movement of one or more fibers. The transition phase is as crucial as the other phases; in fact, the fiber rearrangement, interactions and deformations occur simultaneously. Therefore, the numerical model must be able to reproduce, as closely as possible, these micro-mechanisms compared to the real compaction test. Based on the results from figure 12(a, b), the proposed model seems to reliably simulate the transition phase since the numerical compaction curve is in accordance with the experimental data.

When the displacement reaches the value $U = 1.12mm$, the penalty work increases by almost 92% to its peak value, as shown in figure 13. Before reaching static equilibrium, the fiber network passes through a metastable state. Therefore, fiber interaction increases, causing an increase in the penalty work. Afterwards, a rearrangement of the fibrous microstructure takes place and a stable equilibrium is reached, which explains the decrease in the penalty work and the slight decrease observed in the compaction load (≈9.8%) in both figures 15(a, b) at $U = 1.12mm$. Both parallel and oblique contact models give similar and accurate results concerning the rearrangement phase $U \in [0,0.55]$, and the transition phase $U \in [0.55,1.12]$. Although the impact of fiber-fiber contacts during these two phases is non-negligible, it remains insufficient to cause a noticeable difference between the two contact models. However, a difference is observed concerning the final compaction load: The value predicted by the parallel contact model is 30% higher, and the value predicted by the oblique contact model is 19% lower (for the average value $\Phi_2 = 6°$) than the maximum experimental value. As explained earlier, the average angle was chosen

here for the simulation because: tested three extreme cases ($\Phi_2 = 2°, 6°, 10°$)) and the simulation results were approximated for each direction. Both contact cases are present within the fiber network due to the permanent change in the contact angle between two neighboring fibers, but this variation is very small. Therefore, considering only one contact case cannot model the effect of both contact cases together. However, it is important to recall that fiber assemblies of hundreds of fibers are targeted in further studies. Hence, in order to predict the exact experimental final compaction load the contact angle change needs to be taken into account, which would be expensive in terms of realization and CPU time. Therefore, it is possible to choose the average angle for subsequent simulations as a cost-saving option without introducing large errors. Instead, the proposed contact models with the proposed simulation strategy provides reasonable results in a total CPU time of 14mn42s for 40 fibers. Furthermore, the proposed model can be pushed further by identifying the contact parameters (S, S_0 and d) in order to reduce the difference between the numerical final compaction load and the experimental one. The compaction curve obtained is displayed in figure 12(c) where the difference is reduced to almost 11%. The identified parameters (cf. table 3) lead logically to a contact behavior within the zone between parallel contact and oblique contact behaviors as presented in figure 14. This shows that it is worthwhile investigating in greater depth in further studies and searching for a general contact model in order to combine both parallel and oblique contact behaviors.

Although the developed model obtained by X-ray tomography predicts the same macroscopic behavior as the one obtained experimentally, the microscopic behavior should also be verified by comparing with the experimental results. To verify the accuracy of the initial fiber bundle model, gravity is added to it and only the effect of gravity on the fiber bundles is considered. As shown in the figure 15, comparing the real positions of the fiber bundles after adding gravity in the initial state, the change is negligible. The volume fraction of the initial state of the fiber bundle used for the experiment is 37.7%, which is calculated by MATLAB: the total volume of the fiber bundle divided by the volume of the compression cassette in which the fiber bundle is located. Thus, the model can be further simulated for compression experiments.

The results of compaction test are presented in figure 16 where the fiber positions predicted by the model are compared with their real positions during the compaction test. In addition, quasi-parallel fibers have

a certain curvature. The average curvature projected on XY and YZ plane of fiber bundle in its initial state (at U=0mm) and after compaction (at U=1.15mm) was calculated by MATLAB as shown in the table 4. It can be seen that the curvature of the aligned parallel fiber bundles in the compression experiment has little effect. The results already be applied to simulations: the movement is locked in the fiber orientation (Boundary Conditions), which will more closely resemble the experimental results. Concerning the earlier stages of compaction (the second stage, i.e. $U = 0.21mm$, is taken as an example), the experimental and numerical positions of the fibers seem to be very close, the mean distance between simulation and experiment is 0.32 mm, in the finally state, which is 60% of the fiber's diameter. At further levels of compaction (e.g. $U = 0.58mm$ at the eighth stage) the marginal error between the fibers will normally increase progressively, yet, it does not exceed the fiber diameter (0.5mm). At the final stage of compaction ($U = 1.15mm$), the fibers have regained their experimental position. In fact, as the fiber volume fraction increases, the fibers rearrange and converge to the experimental microstructure. Taking into account the difficulties of simulation at the fiber scale and the assumptions made, the experimental/numerical positions and orientations of the fibers can be considered accurate. The microscopic positions of the fibers can definitely be improved further, but they are accurately controlled. Furthermore, since the numerically predicted compaction curve is very close to the experimental one, this difference in the fiber position does not appear to have a significant effect on the behavior of the fiber network. In other words, a controlled disturbance of the fiber network microstructure does not significantly change its macroscopic behavior.

5 Conclusion

A numerical model has been proposed to simulate the compaction of quasi-parallel fiber assemblies at the fiber scale. A compaction test of forty polyester fibers was performed to enrich the development of a simulation strategy and validate the numerical results. The fiber assembly microstructure was reconstructed from the X-ray tomography images of the real specimen. A CAD model was then obtained, automatically and directly, from the input images, then used afterwards to simulate the compaction test based on the simulation strategy developed. This strategy includes the choice of the finite elements, the analysis platform, the fiber contact law and the analysis parameters to ensure an accurate fiber

rearrangement. Beam finite elements were chosen to model the fibers and optimize the calculation cost. The dynamic explicit analysis in Abaqus/explicit appears to be compatible with the characterization of fibrous media, which include a large number of contacts. The normal contact behavior between the fibers was accurately modelled using the contact stiffness scaling. This method seems to be suitable for the beam's rigid cross-section, but it cannot take into consideration the permanent change of the fibers' relative orientations. However, the alternative solution proposed of using one average relative orientation gives an accurate contact behavior. The contact tangential behavior was also modelled through the Coulomb friction model, and accurate fiber rearrangements were obtained using an appropriate material-damping coefficient.

The simulation strategy has been validated by comparing the mechanical response of the compaction experiment with the numerical one. The proposed model offers encouraging results in accordance with the real compaction test. In addition, the total CPU time of the compaction simulation is 14min42s for forty fibers, which is promising for the integration of more fibers (hundreds of fibers are targeted in further work). The proposed numerical method is directly related to the real microstructure evolution of the fiber assembly. Therefore, it can be used to predict, non-exhaustively, the fiber orientations and kinematics, the influence of friction on the rearrangement, the fiber-fiber interactions and other features that are difficult to explore experimentally at the fiber scale. More loading trajectories will be performed on a bundle of hundreds of fibers to gather more information at the microscopic scale (fiber scale), and then formulate a mechanical behavior at the mesoscopic scale (yarn scale).

Data Availability Statements

All data generated or analysed during this study are included in this published article (and its supplementary information files).

Statements and Declarations

Competing of Interest

The authors declare that they have no known competing financial interests or personal relationships that could have appeared to influence the work reported in this paper and publication of this article.

Acknowledgments

This work of the project supported by the China Scholarship Council (CSC), the project of "National constructed high-level university-sponsored graduate programs" (Funding number: 202008120116).

The authors also thank ANR AMOC and Tec21 for their support.

Appendix: The static case

In order to find the magnitude of $\overrightarrow{\boldsymbol{NF}}$ and $\overrightarrow{\boldsymbol{RF}}$ (figure 11(a)), the static equilibrium is applied as follows.

- The isolated groups.

Let $G1 = \{beam1, beam2, beam3\}$ be the first isolated group and $G2 = \{beam2\}$ the second isolated group. $G1$ is subjected to the reaction forces $\overrightarrow{\boldsymbol{RF_z}}$ and $\overrightarrow{\boldsymbol{RF_z}'}$ applied by the analytical plate along the z-axis, $\overrightarrow{\boldsymbol{RF_y}}$ and $\overrightarrow{\boldsymbol{RF_y}'}$ applied by the analytical plate along the y-axis, the load $\vec{\boldsymbol{q}}$ along the z-axis and the weight $\vec{\boldsymbol{w}}$. $G2$ is subjected to the normal force $\overrightarrow{\boldsymbol{NF}}$ applied by beam 1 along the vector $\vec{\boldsymbol{n}}$, and the reaction forces $\overrightarrow{\boldsymbol{RF_z}}$ and $\overrightarrow{\boldsymbol{RF_y}}$ applied by the analytic rigid plate respectively along the z-axis and the y-axis.

- Application of the static equilibrium:

The equations (A.1) and (A.2) bellow satisfies the static equilibrium of both isolated groups $G1$ and $G2$ respectively.

$$2\overrightarrow{RF_z} + 3\vec{w} + \vec{q} = \vec{0} \tag{A.1}$$

$$\overrightarrow{RF_y} + \overrightarrow{RF_z} + \overrightarrow{NF} + \vec{w} = \vec{0} \tag{A.2}$$

- Scalar projections of equation (A.1) and (A.2) on the x-axis and the z-axis**:**

The static equilibrium of G1 is projected on the z-axis as formulated in equation (A.3), and the static equilibrium of G2 is projected on the y-axis and the z-axis as formulated respectively in equation (A.4) and (A.5).

$$2RF_z - 3w - q = 0 \tag{A.3}$$

$$RF_z - NF\cos(\beta) - w = 0 \tag{A.4}$$

$$-RF_y + NF\ sin(\beta) = 0 \tag{A.5}$$

Basing on equations (A.3), (A.4) and (A.5), the analytical expressions of both normal force NF and reaction force RF_y and $RF_z$are expressed as follows.

$$NF = \frac{q + w}{2\cos(\beta)} \tag{A.6}$$

$$RF_y = \frac{1}{2}(q + w)\tan(\beta) \tag{A.7}$$

$$RF_Z = \frac{1}{2}(q + 3w) \tag{A.8}$$

References

1. C. Picu, "Mechanics of random fiber networks - a review", *Soft Matter,* vol. 7, p. 6768–6785, 2011.
2. D. Poquillon, B. Viguier and E. Andrieu, "Experimental data about mechanical behaviour", *Mechanical Behavior of Cellular,* vol. 40, p. 5963–5970, 2005.
3. A. Janghorban, D. Poquillon, B. Viguier and E. Andrieu, "Compression de fibres enchevêtrées", *Matériaux,* 2006.
4. J. Masse, L. Salvo, D. Rodney, Y. Bréchet and O. Bouaziz, "Influence of relative density", *Scripta Materialia,* vol. 54, p. 1379–1383, 2006.
5. P. Latil, L. Orgéas, C. Geindreau, P.J.J. Dumont and S. Rolland du Roscoat, "Towards the 3d in situ characterisation of deformation micro-mechanisms within a compressed bundle of fibres", *Composites Science and Technology,* vol. 71, pp. 480-488, 2011.
6. M. Alkhagen, and S. Toll, "Micromechanics of a compressed fibre mass", *Journal of Applied Mechanics,* vol. 74, p. 723–731, 2007.
7. P. Badel, E. Vidal-Sallé, E. Maire and P. Boisse, "Simulation and tomography analysis of textile composite reinforcement deformation at the mesoscopic scale", *Composites Science and Technology,* vol. 68, p. 2433–2440, 2008b.
8. D. Rodney, M. Fivel and R. Dendievel, "Discrete modeling of the mechanics of entangled", *Physcal Review Letter,* vol. 95, p. 1–4, 2005.
9. C. Barbier, R. Dendievel and D. Rodney, "Numerical study of 3d-compressions of entangled", *Computational Materials Science,* vol. 45, p. 593–596, 2009.
10. G. Subramanian and C. Picu, "Mechanics of three-dimensional, nonbonded random fiber", *Physical Review E,* vol. 83, pp. 1-9, 2011.
11. S. Heyden, Network modelling for the evaluation of mechanical properties of cellulose fibre fluff, Sweden: Ph.D. thesis, Lund University, 2000.
12. A. Abd El-Rahman and C. Tucker, "Mechanics of random discontinuous long-fiber thermoplastics. Part II: Direct simulation of uniaxial compression", *Journal of Rheology ,* vol. 57, pp. 1463-1489, 2013.
13. C.M.van Wyk, "Note on the compressibility of wool", *Journal of Textile Institute,* vol. 37, pp. 85-92, 1964.
14. S. Toll, "Packing mechanics of fiber reinforcements", *Polymer Engineering and Science,* vol. 38, p. 1337–1350, 1998.
15. D. Durville, "Numerical simulation of entangled materials mechanical properties", *Journal of Materials Science,* vol. 40, p. 5941–5948, 2005.
16. D. Durville, "Simulation of the mechanical behavior of woven fabrics at the scale", *The international journal of material forming,* vol. 3, p. 1241–1251, 2010.
17. N. Beil and W. Roberts Jr., "Fibrous assemblies: Modeling/computer simulation of compressional behaviour", *International journal of clothing science and technology,* vol. 16, p. 108–11, 2004.
18. N. Beil and W. Roberts Jr, "Modeling and computer simulation of the compressional behavior of fiber assemblies. Part I: Comparison to van Wyk's theory",*Textile research journal,* vol. 72, p. 341–351 , 2002a.
19. N. Beil and W. Roberts Jr., ""Modeling and computer simulation of the compressional behavior of fiber assemblies. Part II: Hysteresis, crimp, and orientation effects", *Textile research journal ,* vol. 72, p. 375–382 , 2002b.
20. F. Chatti, C. Bouvet, D. Poquillon and D. Michon, "Numerical modelling of shear hysteresis of entangled cross-linked carbon fibres intended for core material", *Computational Materials ,* vol. 155, pp. 350-363, 2018.
21. F. Chatti, D. Poquillon, C. Bouvet and G. Michon, "Numerical modelling of entangled carbon fibre material under compression", *Computational Materials Science,* vol. 151, pp. 14-24, 2018.
22. D. Rodney, B. Gadot, O. Martinez, S. Rolland du Roscoat and L. Orgéas, "Reversible dilatancy in entangled single-wire materials", *Nature Materials,* vol. 15, p. 72, 2015.

23. C. P. Laurent, P. Latil, D. Durville, R. Rahouadj, C. Geindreau, L. Orgéas and J.-F. Ganghoffer, "Mechanical behaviour of a fibrous scaffold for ligament tissue engineering: Finite elements analysis vs. X-ray tomography imaging", *Journal of the Mechanical Behavior of Biomedical Materials,* vol. 40, pp. 222-233, 2014.
24. N. Moustaghfir, S. El-Ghezal Jeguirim, D. Durville, S. Fontaine and C. Wagner-Kocher, "Transverse compression behavior of textile rovings: finite element simulation and experimental study", *Journal of Materials Science,* vol. 48, pp. 462-472, 2013.
25. G. Zhou, X. Sun, Y. Wang, "Multi-chain digital element analysis in textile mechanics", *Composites Science and Technology,* vol. 64, pp. 239-244, 2004.
26. Y.Miao, E. Zhou, Y.Wang, A.Cheeseman, "Mechanics of textile composites: Micro-geometry", *Composites Science and Technology,* vol. 68, pp. 1671-1678, 2008.
27. L. Daelemans, S. Heijden and I.D.Baere, "Using aligned nanofibres for identifying the toughening micromechanisms in nanofibre interleaved laminates", *Composites Science and Technology,* vol. 124, pp. 17-26, 2016.
28. Abaqus 6.14 Analysis User's.
29. C. Pereira, A. Ramalho and J. Ambrósio, "A critical overview of internal and external cylinder contact force models", *Nonlinear Dynamics,* vol. 63, p. 681–697, 2011.
30. K. Johnson, Contact Mechanics, Cambridge University Press, 1985.
37. B. Cornelissen, The role of friction in two mechanics, PhD Thesis, University of Twente, Enschede, The Netherlands, 2012.
32. H. Gassara, Développement de nouvelles méthodes de mesure du frottement transversal entre fibres, PhD Thesis, Université de Haute Alsace, Fance, 2016.

Figures

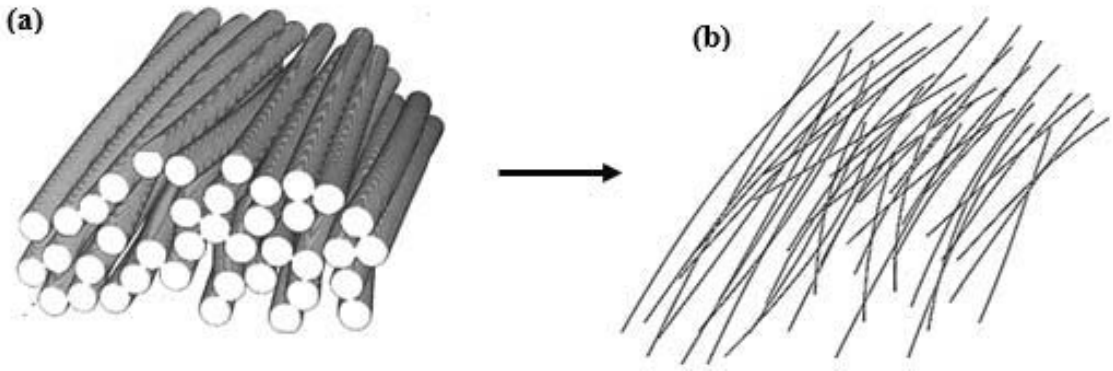

Figure 1: (a) 3D X-ray tomography image of the fiber network specimen in its initial state. (b) The geometry model of the fiber network specimen consists of the fiber mid-lines

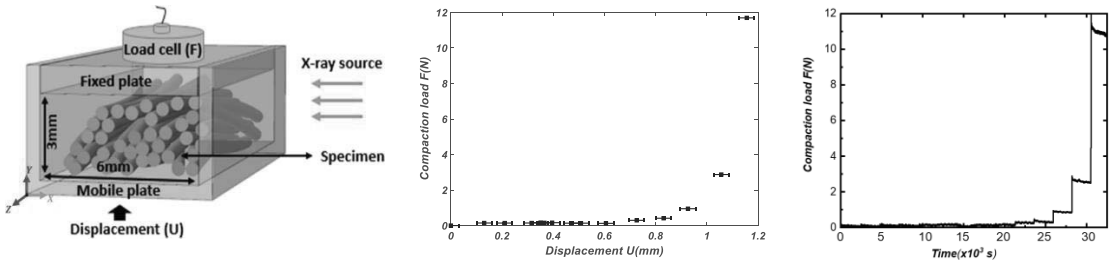

(a) Scheme of the compaction test

(b) Evolution of the compaction load F as a function of the lower plate displacement U

(c) Evolution of the compaction load F as a function of the lower plate time

Figure 2: The uniaxial confined compaction test

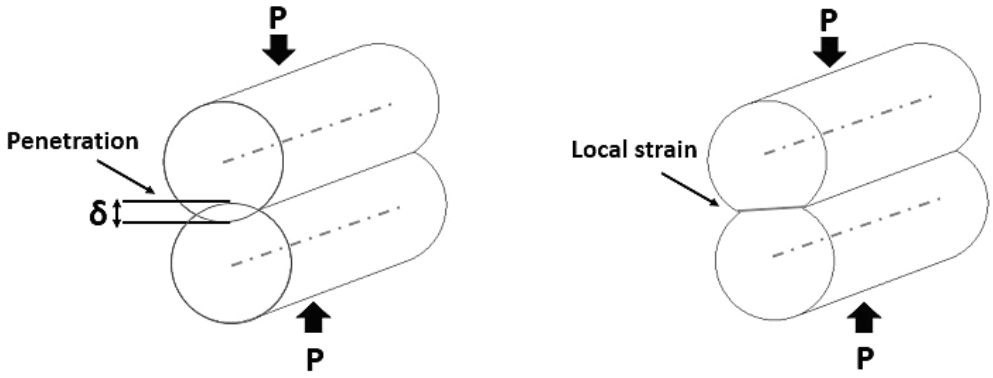

(a) Rigid cross-section *(b)Deformable cross-section*

Figure 3: Contact behavior depending on the deformability of the cross-section

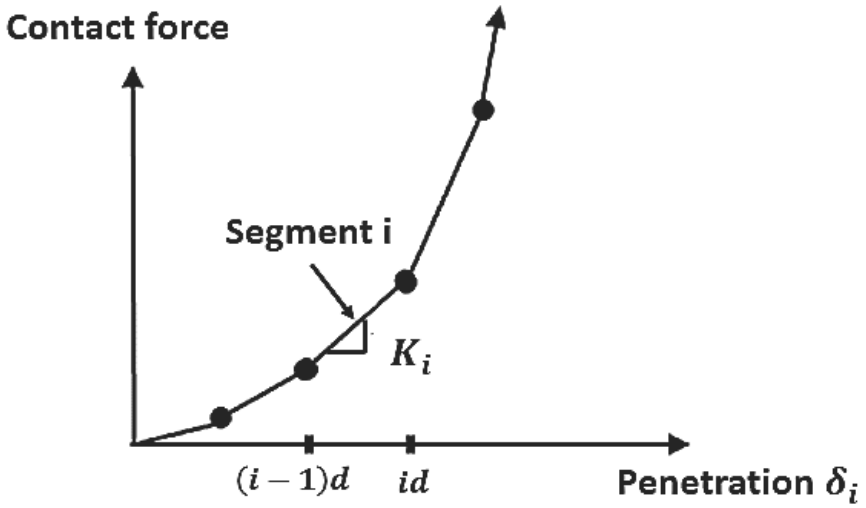

Figure 4: Simulation contact model: scale factor contact force-penetration relationship [29].

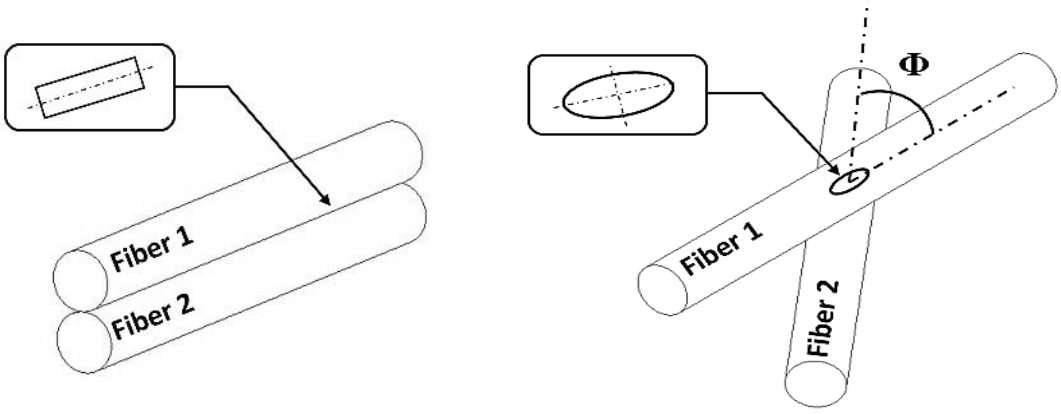

(a) Parallel contact model *(b) Oblique contact model*

Figure 5: The contact models

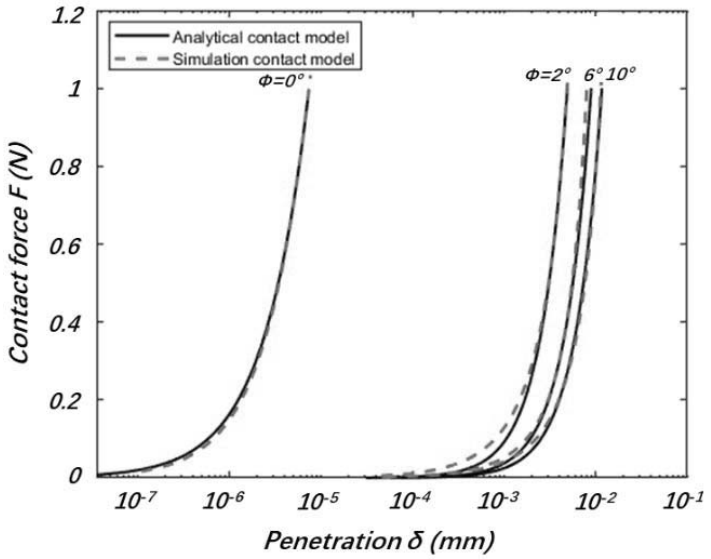

Figure 6: Identification of the simulated parallel (Φ=0°) and three different oblique contact model given by the analytical models (n ≈1000)

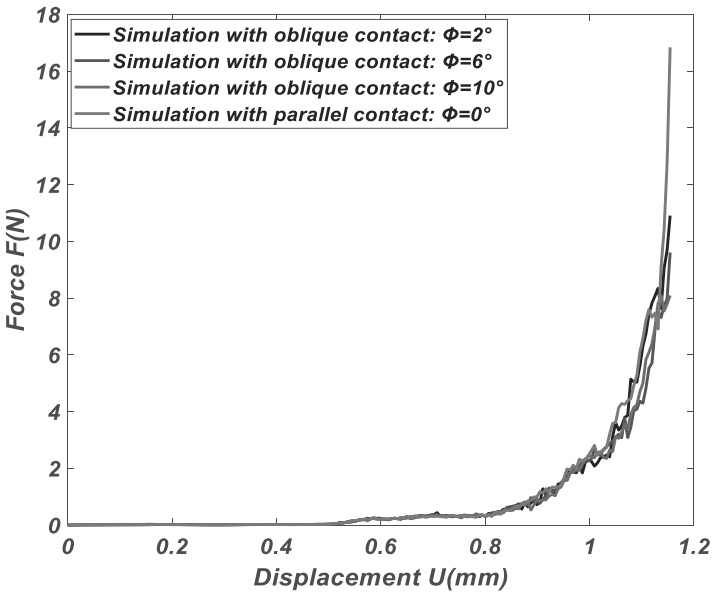

Figure 7: Simulation of the compaction test using the parallel contact model and the oblique contact model with three identified relative orientations

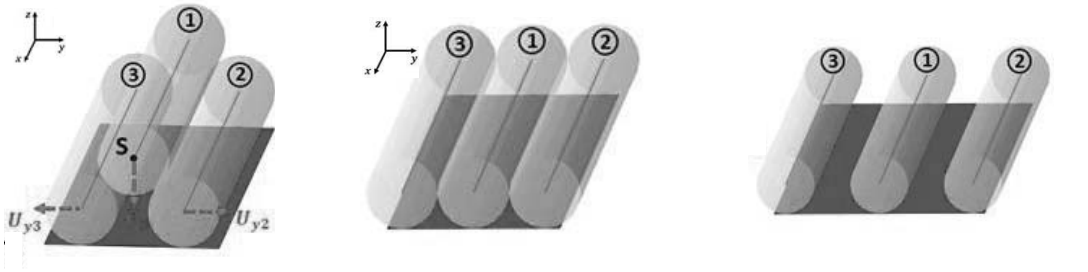

(a) Initial state

(b) Quasi-static rearrangement obtained by a dynamic implicit analysis: reference solution, v_z=0.23mm/min

(c) Rearrangement obtained by the explicit dynamic analysis with inertia effects and contact loss, v_z=1000mm/min, CPU time=27min

Figure 8: Test case: rearrangement of three straight and parallel 3D beams

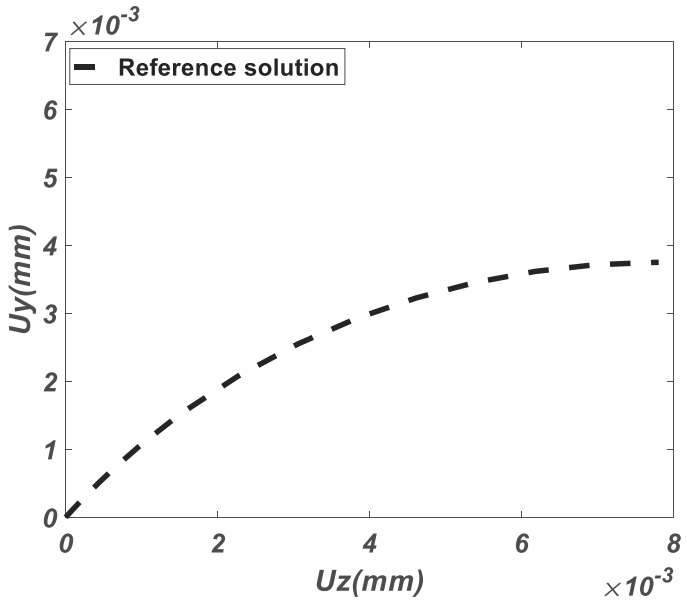

Figure 9: Test case: the reference solution of the displacement U_y obtained by the dynamic implicit analysis

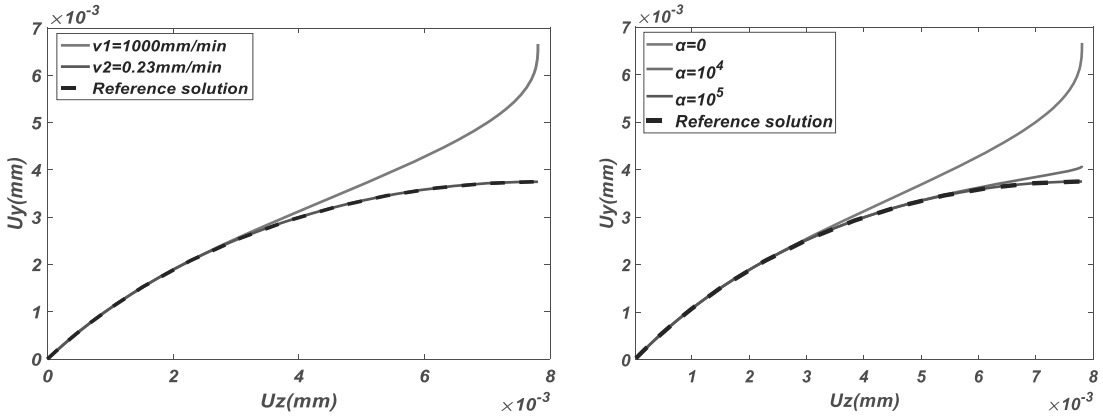

(a) Influence of the velocity

(b) Influence of material damping on fiber rearrangement for v_z=1000mm/min.

Figure 10: Influence of parameters on the fiber rearrangement

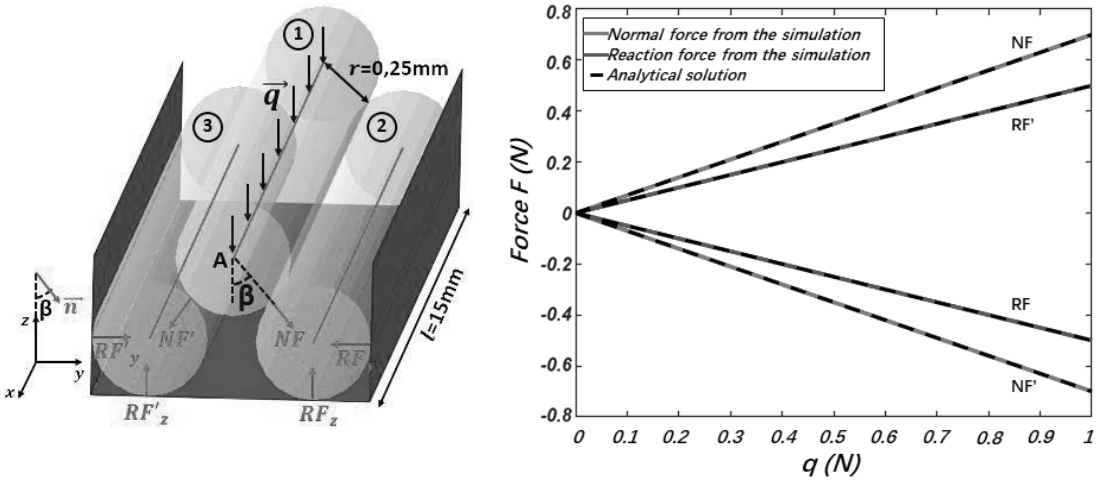

(a) the static case

(b) Evolution of normal contact force (NF and NF') and reaction force (RF and RF') as a function of the compaction load q

Figure 11: Contact between three straight parallel beams

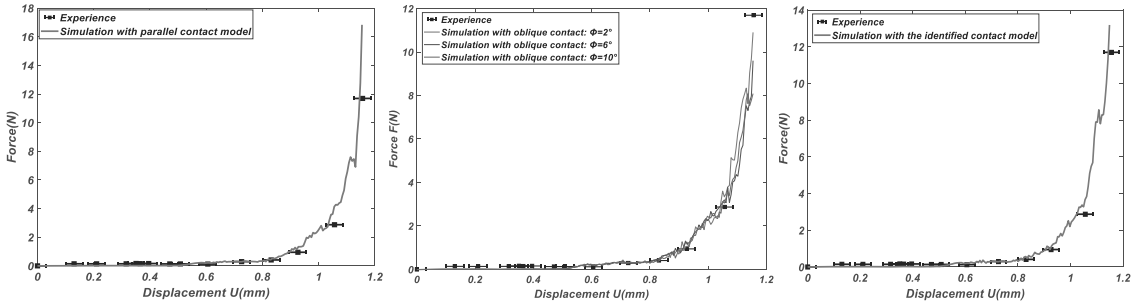

(a) the parallel contact model

(b) the oblique contact model of three different relative orientations

(c) the identified contact model

Figure 12: Experimental compaction test compared to the compaction simulation obtained with

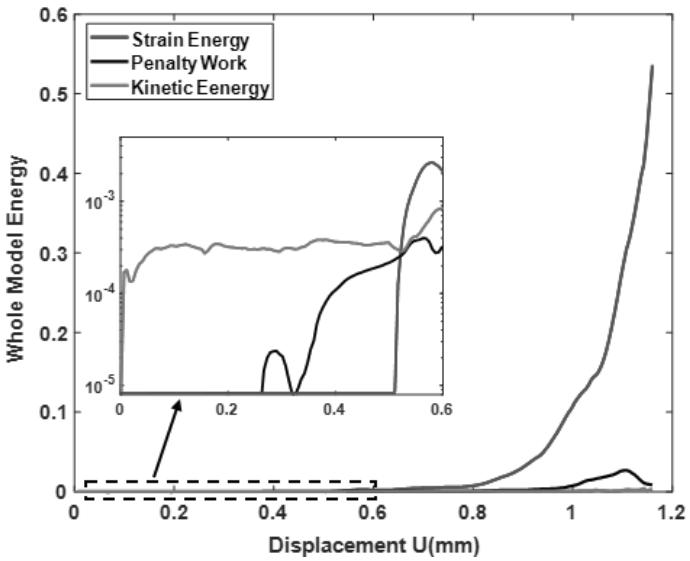

Figure 13: The Whole model strain energy, penalty work and kinetic energy during the compaction simulation

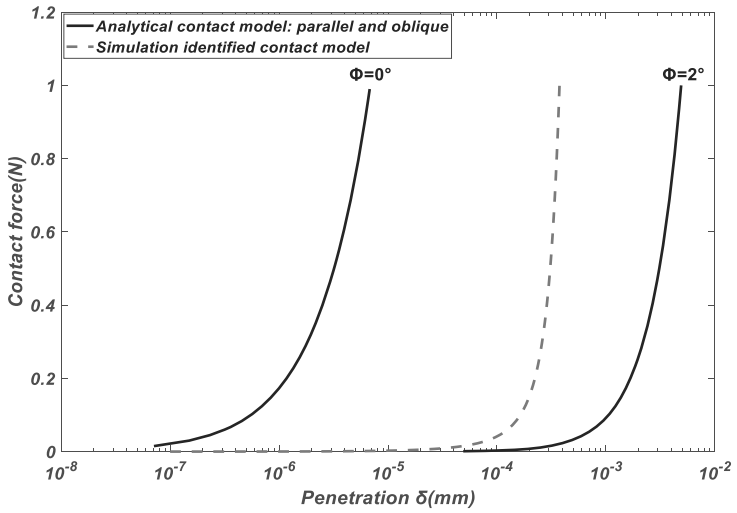

Figure14: The identified contact model compared to the parallel and the oblique analytical contact models

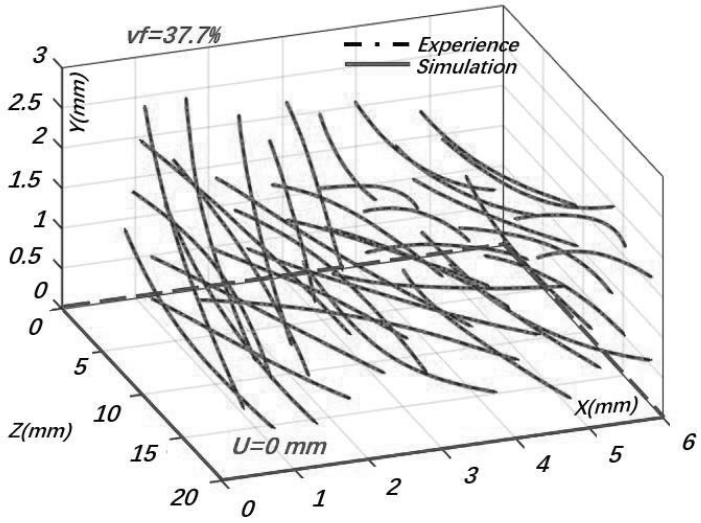

Figure 15: Fiber positions with gravity in the developed model compared with their real position in the initial compaction test (with the volume fraction=37.7% in the initial experiment state)

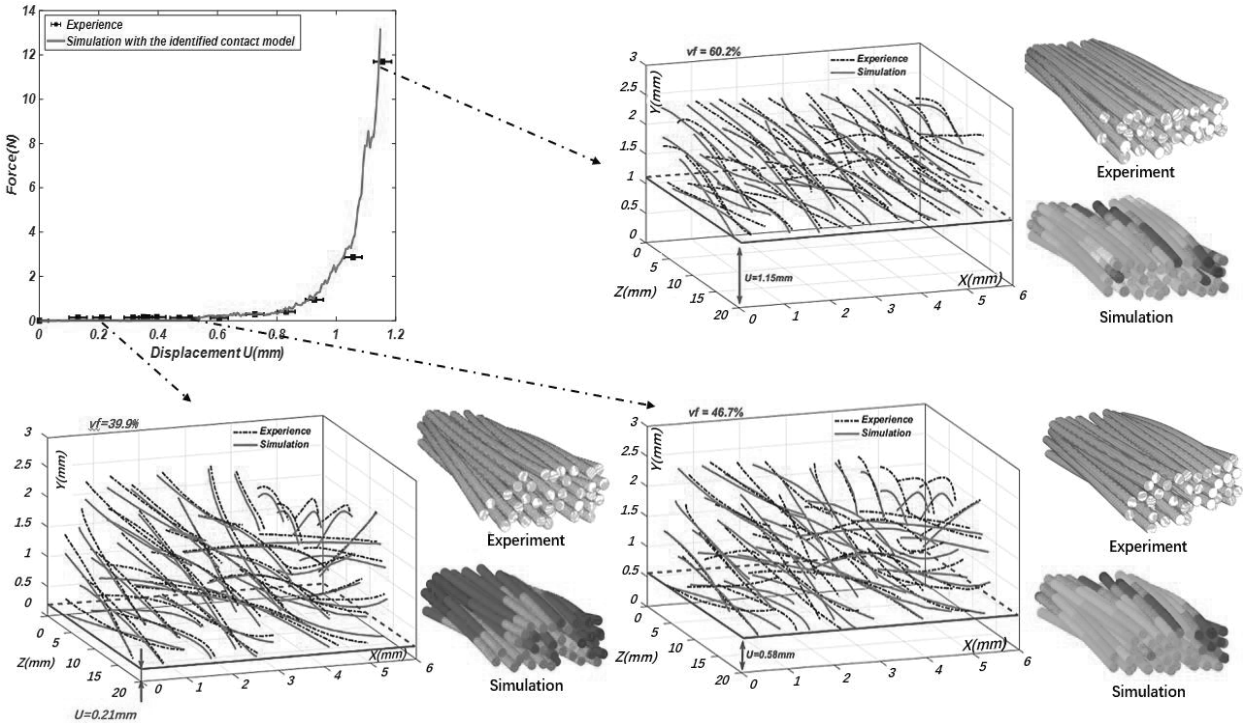

Figure 16: Fiber positions predicted by the developed model compared with their real positions (with the different volume fraction in the experiment) during the compaction test

Tables

Φ	d **(mm)**	S	S_0
0°	1.10^{-7}	1.0008	0.74
2°	$4{,}6.10^{-5}$	1.0101	0.021
6°	$4{,}6.10^{-5}$	1.0047	0.0087
10°	5.10^{-5}	1.0045	0.013

Table 1: The simulation contact parameters given by the analytical models

α	0	10^4	10^5
CPU time (s)	27	30	34

Table 2: Influence of material damping on the CPU time of the test case in figure 8

d **(mm)**	S	S_0
1.10^{-7}	1.001	0.05

Table 3: The simulation contact parameters of the identified contact model

Displacement	Projected average curvature (m^{-1})	
	XZ-plane	YZ-plane
U=0mm	*0.241*	*0.248*
U=1.15mm	*0.228*	*0.221*

Table 4: The average curvature projected on the XY and YZ plane in the initial and finial state of compaction.